# *Modelling Fluid Loss Faults in Piezoresistive Pressure Sensors*

Kamran Soltani
Mechanical Engineering Department
Urmia University, Urmia, Iran
kamransoltani16377@gmail.com

Manus Patrick Henry
University of Oxford, Oxford, GB
Coventry University, Coventry, GB
South Ural State University, Chelyabinsk, Russian Federation
manus.henry@eng.ox.ac.uk

Mina Ghanbari
Mechanical Engineering Department
Urmia University, Urmia, Iran
m.ghanbari@urmia.ac.ir

Ekatrina Tugova
South Ural State University, Chelyabinsk, Russian Federation
e.tugova@...

Oleg Bushuev
South Ural State University, Chelyabinsk, Russian Federation
oleg.u.bushuev@gmail.com

Ghader Rezazadeh
Urmia University, Urmia, Iran
South Ural State University, Chelyabinsk, Russian Federation
g.rezazadeh@urmia.ac.ir

*Abstract*— **The efficient operation of industrial processes requires the timely and accurate diagnosis of faults in process equipment, particularly sensors, as acting on faulty measurement data can result in inefficient or dangerous operation. A common fault mode in industrial pressure sensors is mechanical damage resulting in the leakage of the internal oil (used to transmit external pressure to the sensing element) and the development of an air pocket within the device. In previous work, we have experimentally determined the faulty measurement characteristics of a commercial pressure sensor, where the sensor manufacturer has provided modified sensors with calibrated degrees of oil loss. The current paper develops a mathematical model of this tenso-resistive pressure sensor, which describes and explains the impact that oil loss, and hence the presence of an air pocket, has on the static measurement response.**

**Keyword**

## I. INTRODUCTION

Pressure is a key parameter when investigating the thermodynamics properties of physical phenomenon. Accordingly, pressure measurement is essential in many applications where pressure itself play an important role [1]. Pressure transmitters (pressure sensors) are widely used in a range of industrial processes including automotive, industrial, aerospace, biomedical etc. [2–4]. Manometers, diaphragms and bourdon tubes were the first class of measuring pressure instruments, and were based on converting the magnitude of the applied pressure to a mechanical deflection of an indicator [5]. Technological progress led to the appearance of new pressure measurement devices in which the externally applied pressure (input pressure) is directly converted into an electrical output signal; these transmitters types are called mechanical-electrical transducers [5,6]. It should be noted that in the present paper the terms, "sensor", "transmitter" and "transducer" are used interchangeably, given the integrated nature of industrial pressure products.

Today, many different types of pressure sensors are utilized, including tenso or piezo-resistive (also called strain gauge) [3–7], piezoelectric [8,9], capacitive [3,4], resonant [10,11] and optical fiber [12,13]. Each pressure sensor type is based on a physical property such as resistance, capacitance, electrical charge, etc. with its characteristic advantages and limitations.

Piezoelectric pressure sensors are utilized for measuring highly dynamic pressure. The working principle is based on the piezoelectric effect, i.e. the property of materials that produce electrical charge when subjected to mechanical stress, and conversely, voltage applied to these materials leads to stress and consequently deflection in shape. Commonly used materials for piezoelectric pressure transmitters are PZT, BiFeO3, and ZnO [14,15].

Capacitive pressure transmitters detect capacitance change caused by relative movement between the parallel plates of a capacitor due to applied pressure. Increasing pressure reduces the distance between the parallel plates, and the resulting capacitance change is a function of the sensor design parameters. In optical pressure sensors, an optical fiber and the pressure diaphragm are connected via capillary tubing. Light from a section of the fiber is reflected by a small interferometer. A movable film made of silica glass, SiO2, or graphene is deformed by the applied pressure [16–20].

In resonant pressure sensors, pressure applied to the sensing element adjusts the oscillation frequency of a resonator. Typically, a resonant beam is suspended on a pressure-sensitive silicon diaphragm. The resonator is excited via a magnetic or electric field and the resonant

frequency is detected using an inductive voltage. The pressure-sensitive diaphragm is deformed by the applied pressure, which causes tensile and compressive stress to act on the resonator [10,11].

Of the various types of pressure sensors, tenso-resistive devices have several attractive properties such as high sensitivity, a simple physical model and fabrication, high accuracy, low cost, a strong output signal and low drift; these properties make them a good choice in many industrial measurement applications [6]. Piezoresistive pressure transmitters fall into several subcategories based on the material utilized for piezo-resistors [21,22], the material used for the plates (diaphragms) [22–24], the wafer type [25], the method of micromachining the diaphragms [23], as well as the type of pressure measured by the transmitter (e.g. absolute or gauge). The working principle of piezoresistive transmitters is that variation in the applied pressure causes a corresponding change in electrical resistance. Electrical resistance is also utilized in many other measurement devices such as inertial sensors, accelerometers, strain gauges and cantilever force sensors [26]. Piezoresistive pressure sensors typically include a flexible diaphragm or plate, which is deflected by a mechanical loading (pressure) applied on it. In the design considered here, pressure applied to a relatively soft external diaphragm (called the membrane) is transferred to another stiffer plate (the sensing plate) via an incompressible fluid. The incompressible fluid between the membrane and sensing plate (known as interface fluid) is usually a silicone oil. The stiffer plate supports several strain gauges which measure plate deflection, generating a proportional electrical signal. Figure (1a) illustrates a two-plate piezoresistive transmitter. A restriction may be applied on the maximum deflection of the membrane to prevent its plastic deformation, resulting in a limit on the maximum measurable pressure for the device. Any compressibility of the interface fluid leads to measurement error since energy is consumed in compressing the fluid, so that the external pressure is not entirely transferred to the sensing plate.

The present study provides an overview of the main failure modes for piezo-electric pressure sensors. These include temperature effects, loss of the interface fluid, initial deflection of the diaphragms, corrosion, and sudden pressure loss caused by the condensing of gas (often wet air) trapped in the interface volume. For each failure type, mathematical modelling of the static and dynamic behaviour is proposed. However, the main investigation here is concerned with oil loss. To analyse this problem mathematically, transverse motion equations are derived for the membrane and the sensing plate. Should air become trapped in the interface, the governing equations become nonlinear due to compressibility of the air. The system of linear and nonlinear governing equations is solved using the SSL Method [27] combined with weighted residual methods based on the Galerkin approach [28,29]. It should be noted that the air is assumed to be an ideal gas that obeys the gas state law equation.

## 2 Model Description

As noted in the previous section, mechanically the piezoelectric type pressure transmitters consists of three main regions: the membrane (upper diaphragm), the middle volume, which is filled with the incompressible fluid, and the sensing plate (lower, stiffer diaphragm), including the strain gauges which generate the output signal. Figure (1-a) shows the schematic of the pressure sensor for the case where air is trapped in the interface volume due to fluid loss, which may arise due to mechanical damage during industrial operation.

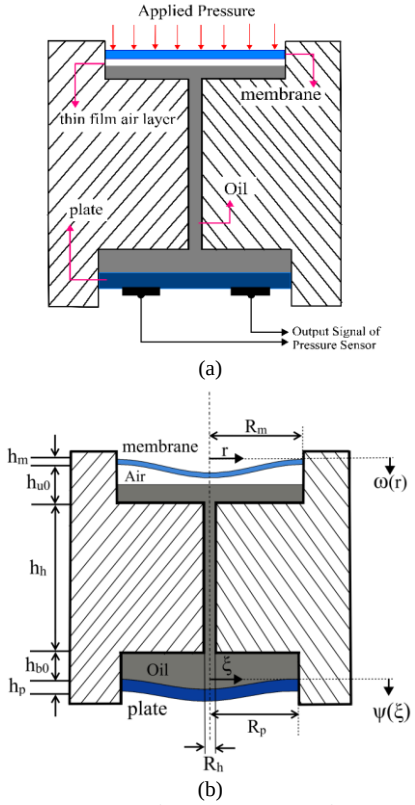


***Fig 1**: A schematic view of the cross-section of the tenso-resistive pressure transmitter.*

## II. Mathematical Modelling of Faluire Modes

### *A. Temperature Effects*

When a mechanical element such as a beam, membrane, plate bar etc. experiences temperature change, thermal stresses are produced. These stresses may lead to phenomenon such as buckling [30,31] or wrinkling of the plate and membrane. The two-plate piezoresistive pressure transmitters are especially vulnerable to this effect because their membranes are usually thin. A related fault mode is where the temperature is high but steady: here the pressure sensor may be stable below a specific pressure, however higher applied pressure may result in membrane instability

(for example by inducing higher modes of transverse motion).

Based on the geometry of the piezoresistive pressure sensor (Figure (1b)), the governing dynamic equations can be written as follows [1,32,33]:

$$D_m\nabla^2\nabla^2 w - \left(\frac{1}{2}\frac{E_m h_m}{(1-\upsilon_m^2)}\int_0^{R_m}\left(\frac{\partial w}{\partial r}\right)^2 dr + \frac{E_m}{1-\upsilon_m}\int_{-\frac{h_m}{2}}^{\frac{h_m}{2}}\varepsilon_{HT}dz\right)\nabla^2 w + \rho_m h_m\frac{\partial^2 w}{\partial t^2} = \hat{P}_{in}(t) - \boldsymbol{P}_{Oil}(r,t) \quad (1)$$

$$D_p\nabla^2\nabla^2 w - \left(\frac{1}{2}\frac{E_p h_p}{(1-\upsilon_p^2)}\int_0^{R_p}\left(\frac{\partial \psi}{\partial \xi}\right)^2 d\xi\right)\nabla^2\psi + \rho_p h_p\frac{\partial^2\psi}{\partial t^2} = \overline{\boldsymbol{P}}_{Oil}(r,t) \quad (2)$$

where $w$ and $\psi$ are the transverse deflections of the membrane and the plate. $E_m$ and $\upsilon_m$ are the elasticity module and the Poisson's ratio of the membrane, respectively (subscript "p" indicates the sensing plate). $h_m$ is the thickness of the membrane. $\hat{P}_{in}$, $\boldsymbol{P}_{Oil}$ and $\overline{\boldsymbol{P}}_{Oil}$ are the external pressure applied to the membrane, the pressure distribution inside the interface volume on the membrane, and the pressure distribution on the sensing plate. $\varepsilon_{HT}$, $D_m$ and $\nabla^2$ are the thermal strain inside the membrane, the flexural rigidity of the membrane and the Laplacian operator, respectively, which can be written as follows:

$$\varepsilon_{HT} = \alpha_T \Delta \mathrm{T} \ , \ D_m = \frac{1}{12}\frac{E_m h_m}{(1-\upsilon_m^2)} \ , \ \nabla^2 = \frac{\partial^2}{\partial r^2} + \frac{1}{r}\frac{\partial}{\partial r} + \frac{1}{r^2}\frac{\partial}{\partial \theta} \quad (3)$$

where $\alpha_T$, is the thermal conductivity coefficient of the membrane and $\Delta T$ is the temperature difference between the membrane and the external environment. It should be noted that the first and second terms inside the parenthesis of Equation (1) are the mid-plane stretching and the thermal force. Equation (1) can be solved in combination with the conduction heat transfer equation, but since the membrane is thin it can be assumed that the temperature gradient is negligible, so that temperature is only a function of time. Also, in a dynamic analysis, the pressure inside the interface fluid is not uniform so that the Navier-Stokes equation should be solved for the fluid domain (for brevity this is not included). In a static analysis, all time dependent terms are removed from equations (1) - (3). The initial and boundary conditions for equation (1) can be summarized as follows:

$$BC:\ w(R_m,t) = \left.\frac{\partial w}{\partial r}\right|_{r=R_m} = 0 \ , \quad \psi(R_p,t) = \left.\frac{\partial \psi}{\partial \xi}\right|_{r=R_p} = 0 \ and \text{ finite values for } w(0,t) \ and \ \psi(0,t) \quad (4)$$

$$IC:\ w(r,0) = \left.\frac{\partial w}{\partial t}\right|_{t=0} = 0 \ , \ \psi(\xi,0) = \left.\frac{\partial \psi}{\partial t}\right|_{t=0} = 0$$

To solve these equations, numerical methods such as the Galerkin weighted residual method combined with FEM method can be applied. It is clear, however, that the solution of the governing equations is not easy and will be investigated in future research.

### *B. Corrosion*

Corrosion is another failure mode which may degrade the performance of the piezoresistive type pressure sensors. This phenomenon gradually destroys the materials (often metals) of the pressure sensor. Corrosion may arise from two main causes: the external fluid may create bubbles on the surface of the membrane, and air bubbles may arise within the interface fluid (fluid loss fault). Mathematical modelling of this fault is beyond the scope of this paper. However, the mathematical-chemical study of corrosion may lead to its prevention and/or techniques for improving the sensor's performance in environments where corrosion is unavoidable.

### *C. Missing Oil*

Oil insufficiency or loss (i.e. a shortage of liquid to fill the interface volume) may arise during the fabrication process or as a result of sensor damage. In an ideal case, the interface volume between the two plates is entirely filled with an incompressible fluid. Missing oil may lead to two possible scenarios: one where air is trapped in the interface volume, and the other where there is a deflection offset caused by a vacuum. In the first scenario, when the chamber is filled with the interface fluid, bubbles may be created, filling a proportion of the middle volume. The focus of the present paper is to analyse the consequences of trapped air in the middle volume. The mathematical modelling is given in the next section. In the second scenario, air is excluded and instead a vacuum is created. To achieve equilibrium, the soft membrane is deflected, even without any applied pressure. The analysis of this initial deflection is very similar to the previously proposed models: the governing equations of a twisted circular membrane, coupled with the equations governing the sensing plate, need to be solved. The resulting behaviour of the sensor is similar to the fault free condition, but the constraint on maximum deflection results in a reduced pressure measurement range; this can be calculated from a static and dynamic analysis. The only difference concerns the initial conditions, which can be written as follows (from equations (1) and (2), with or without temperature-related terms):

$$IC:\ w(r,0) = w_{ini}(r)\ ,\ \ \psi(\xi,0) = \psi_{ini}(\xi) \tag{5}$$

where $w_{ini}(r)$ and $\psi_{ini}$, are the functions describing the initial deflection of the membrane and sensing plate.

*D. Sudden pressure discharge*

In the situation where air bubbles or a thin air layer are present in the interface volume, another potential failure is where high external pressure is applied, resulting in condensation from moist air and a corresponding reduction in volume.

*E. Mathematical modelling of oil loss*

Here we propose a mathematical model for the oil loss failure. From figure (1b), the governing dynamic equations are as follows:

$$D_m\nabla^2\nabla^2 w - \frac{E_m h_m}{1-\upsilon_m^2}\left(\frac{1}{2}\int_0^{R_m}\left(\frac{\partial w}{\partial r}\right)^2 dr\right)\nabla^2 w + \rho_m h_m\frac{\partial^2 w}{\partial t^2} = -\widehat{\boldsymbol{P}}_{\boldsymbol{gas}}(t) + \hat{P}_{in}(t) \tag{6}$$

$$D_p\nabla^2\nabla^2\psi - \frac{E_p h_p}{1-\upsilon_p^2}\left(\frac{1}{2}\int_0^{R_p}\left(\frac{\partial \psi}{\partial \xi}\right)^2 d\xi\right)\nabla^2\psi + \rho_p h_p\frac{\partial^2 \psi}{\partial t^2} = \bar{\boldsymbol{P}}_{\boldsymbol{Oil}}(r,t) + \hat{P}_{atm} \tag{7}$$

$$\widehat{\boldsymbol{P}}_{\boldsymbol{gas}}(t)V_{gas}(t) = n\bar{R}T_{gas} \tag{8}$$

where $\widehat{\boldsymbol{P}}_{\boldsymbol{gas}}$ and $\bar{\boldsymbol{P}}_{\boldsymbol{Oil}}$ are the gas pressure and oil pressure exerted on the membrane and sensing plate, respectively. $V_{gas}$ is the instantaneous volume of the gas. $n$ is the number of moles of gas. $\bar{R}$ is the universal gas constant. $T_{gas}$ is the gas temperature. It is assumed that any pressure change in gradual. From a static perspective, by substituting the gas pressure from equation (8) into equations (6) and (7) and then inserting the gas volume, the equations are simplified as follows:

$$D_m\nabla^2\nabla^2 w - \frac{E_m h_m}{1-\upsilon_m^2}\left(\frac{1}{2}\int_0^{R_m}\left(\frac{\partial w}{\partial r}\right)^2 dr\right)\nabla^2 w = -\frac{n\bar{R}T_{gas}}{V_0 - 2\pi\left(\int_0^{R_m} w(r)rdr - \int_0^{R_p}\psi(\xi)\xi d\xi\right)} + \hat{P}_{in} \tag{9}$$

$$D_p\nabla^2\nabla^2\psi - \frac{E_p h_p}{1-\upsilon_p^2}\left(\frac{1}{2}\int_0^{R_p}\left(\frac{\partial \psi}{\partial \xi}\right)^2 d\xi\right)\nabla^2\psi = \frac{n\bar{R}T_{gas}}{V_0 - 2\pi\left(\int_0^{R_m} w(r)rdr - \int_0^{R_p}\psi(\xi)\xi d\xi\right)} - \hat{P}_{atm} \tag{10}$$

where $V_0$, is the volume of the trapped gas inside the interface volume.

## III. Numerical solution

It is clear from the governing equations (9) and (10) that the physics of the problem is inherently nonlinear. The nonlinearity is caused by the compressibility of the trapped gas as well as the mid-plane stretching that may increase with high deflections of the membrane and plate. The mid-plane stretching is included in the analysis, even though it only has a small effect on the motions of both the sensing plate and membrane over the operational range of pressure sensor.

To overcome the difficulties of the nonlinear equations, conventional linearization is applied. The linearization method is based on Taylor's expansion where the nonlinear terms are linearized about a known point (e.g. initial conditions) of the governing equations. This approach delivers high accuracy for 'small' nonlinearities, where the definition of 'small' depends on the physics of the problem. To extend its range of application, step-by-step linearization (the SSL method) is applied, where the nonlinear terms in each step are linearized about the previous step. This approach has proved to be very effective, especially in the static and quasi static electrostatic problem [27,29,34]. To simplify the form of equations (9) and (10) we define:

$$NT = \frac{n\bar{R}T_{gas}}{\pi R_m^2 g_{air} - 2\pi\left(\int_0^{R_m} w(r)rdr - \int_0^{R_p}\psi(\xi)\xi d\xi\right)}, \qquad T = \nabla^2,\quad L = \nabla^4 \tag{11}$$

Note that the operators $L$ and $T$ are linear. Assuming that the state of the system is known at step $k$ for applied pressure $\bar{p}_{in}^{k}$, the change at step $k+1$ can be approximated using the following linear relations:

$$w^{k+1} = w^k + \delta w = w^k + \phi(r)\ ,\ \psi^{k+1} = \psi^k + \delta\psi = \psi^k + \gamma(\xi) \tag{12}$$

where the pressure is increased by one step:

$$\hat{P}_{in}^{k+1} = \hat{P}_{in}^{k} + \Delta\hat{P}_{in} \tag{13}$$

From definition (11) and the linearized functions for transverse motion and pressure step (equations (12) and (13)), the set of differential equations (9) and (10) at step $k+1$ taken following forms:

$$\begin{cases} D_m L(w^{k+1}) - N_{am}^{k+1}T(w^{k+1}) = -NT^{k+1} + \hat{P}_{in}^{k+1} \\ D_p L(\psi^{k+1}) - N_{ap}^{k+1}T(\psi^{k+1}) = -NT^{k+1} + \hat{P}_{atm} \end{cases} \tag{14}$$

where the axial stretching forces are given by following functions:

$$N_{am}^{k+1} = \frac{E_m h_m}{2(1-\upsilon_m^2)}\int_0^{R_m}\left(\frac{\partial w^{k+1}}{\partial r}\right)^2 dr \tag{15}$$

$$N_{ap}^{k+1} = \frac{E_p h_p}{2(1-\upsilon_{p)}^2}\int_0^{R_p}\left(\frac{\partial \psi^{k+1}}{\partial \xi}\right)^2 d\xi \tag{16}$$

In order to linearize the nonlinear term of the left-hand side of the set of equations ($NT^{k+1}$), using Taylor's series, equation (14) about step $k$ can be rewritten as:

$$NT^{k+1} = \frac{n\bar{R}T_{gas}}{V_0 - \left(\Delta V_m^k - \Delta V_p^k\right)} + \frac{n\bar{R}T_{gas}(\Delta V_m^{k+1} - \Delta V_m^k)}{\left(V_0 - \left(\Delta V_m^k - \Delta V_p^k\right)\right)^2} - \frac{n\bar{R}T_{gas}\left(\Delta V_p^{k+1} - \Delta V_p^k\right)}{\left(V_0 - \left(\Delta V_m^k - \Delta V_p^k\right)\right)^2} + \cdots \tag{17}$$

$$NT^{k+1} \cong NT^k + \frac{n\bar{R}T_{gas}\delta(\Delta V_m)}{\left(V_0 - \left(\Delta V_m^k - \Delta V_p^k\right)\right)^2} - \frac{n\bar{R}T_{gas}\delta\left(\Delta V_p\right)}{\left(V_0 - \left(\Delta V_m^k - \Delta V_p^k\right)\right)^2} \tag{18}$$

where $\Delta V_m^{k+1}$ and $\Delta V_p^{k+1}$ are variations of the interface volume associated with the deflection of the membrane and sensing plate at step $k+1$. Also, $\delta(\Delta V_m)$ and $\delta(\Delta V_p)$, can be determined using the theory of calculus of variations as follows:

$$\delta(\Delta V_m) = 2\pi \int_0^{R_m} \delta w r dr = 2\pi \int_0^{R_m} \phi(r) r dr \tag{19}$$

$$\delta\left(\Delta V_p\right) = 2\pi \int_0^{R_p} \delta\psi \xi d\xi = 2\pi \int_0^{R_p} \gamma(\xi)\xi d\xi \tag{20}$$

The nonlinear stretching term can be linearized by applying Taylor's expansion about the previous step (step $k$), yielding:

$$N_{am}^{k+1}T(w^{k+1}) = N_{am}^k T(w^k) + N_{am}^k T\left(\phi(r)\right) + \delta N_{am} T(w^k) + \delta N_{am} T\left(\phi(r)\right) \tag{21}$$

$$N_{ap}^{k+1}T(\psi^{k+1}) = N_{ap}^k T(\psi^k) + N_{ap}^k T\left(\gamma(\xi)\right) + \delta N_{ap} T(\psi^k) + \delta N_{ap} T\left(\gamma(\xi)\right) \tag{22}$$

where the variations of the axial force ($\delta N$) for small increasing step of pressure ($\Delta\hat{P}_{in}$) can be neglected, so that the left-hand sides are also linearized. By applying the theory of calculus of variations, changes in the axial stretching forces are obtained as follows:

$$\delta N_{am} = \frac{E_m h_m}{1 - \upsilon_m^2} \int_0^{R_m} \left(\frac{\partial w}{\partial r}\right)\Big|_{w=w^k} \left(\frac{\partial \phi}{\partial r}\right) dr \tag{23}$$

$$\delta N_{ap} = \frac{E_p h_p}{1 - \upsilon_p^2} \int_0^{R_p} \left(\frac{\partial \psi}{\partial r}\right)\Big|_{\psi=\psi^k} \left(\frac{\partial \gamma}{\partial \xi}\right) d\xi \tag{24}$$

Substituting equations (22) to (26) into the system of equations (14) leads to the following form:

$$D_m L\left(\phi(r)\right) - \left(N_{am}^k T\left(\phi(r)\right) + \delta N_{am} T(w^k)\right) = -2\pi H^k \int_0^{R_m} \phi(r) r dr + 2\pi H^k \int_0^{R_p} \gamma(\xi)\xi d\xi + d\hat{P}_{in} \tag{25}$$

$$D_p L\left(\gamma(\xi)\right) - \left(N_{ap}^k T\left(\gamma(\xi) + \delta N_{ap} T(\psi^k)\right)\right) = 2\pi H^k \int_0^{R_m} \phi(r) r dr - 2\pi H^k \int_0^{R_p} \gamma(\xi)\xi d\xi \tag{26}$$

where $H^k$ is defined as:

$$H^k = \frac{n\bar{R}T_{gas}}{\left(V_0 - \left(\Delta V_m^k - \Delta V_p^k\right)\right)^2} \tag{27}$$

Solving equations (27) and (28) is a boundary value problem. Several techniques, such as Galerkin's weighted residual method, finite difference analysis (FEA) etc. can be utilized to solve this problem. In the present paper Galerkin' based weighted residual method is employed for solving the set of boundary value equations. Initially, finite function spaces are selected as follows:

$$\phi(r) = \sum_{i=1}^{N} a_{mi}\mu_i(r) \quad , \quad \gamma(\xi) = \sum_{j=1}^{M} a_{pj}\Omega_j(\xi) \tag{28}$$

where $\mu_i(r)$ and $\Omega_j(\xi)$, are basis functions (or equivalently mode shapes) of the membrane and sensing plate, respectively. Substituting equation (28) into equations (25) and (26), a reduced order model is obtained:

$$\begin{aligned} &\sum_{i=1}^{N} D_m L(a_{mi}\mu_i(r)) - N_{am}^k \sum_{i=1}^{N} T(a_{mi}\mu_i(r)) \\ &- \frac{E_m h_m}{1 - \upsilon_m^2} T(w^k) \sum_{i=1}^{N} a_{mi} \int_0^{R_m} \left(\frac{\partial w}{\partial r}\right)\Big|_{w=w^k} \left(\frac{\partial \mu}{\partial r}\right) dr \\ &= -\sum_{i=1}^{N} 2\pi H^k \int_0^{R_m} a_{mi}\mu_i(r) r dr \\ &+ \sum_{j=1}^{M} 2\pi H^k \int_0^{R_p} a_{pj}\Omega_j(\xi)\xi d\xi + \Delta\hat{P}_{in} + E_1 \end{aligned} \tag{29}$$

$$\begin{aligned} &\sum_{j=1}^{M} D_p L(a_{pj}\Omega_j(\xi)) - N_{ap}^k \sum_{j=1}^{M} T(a_{pj}\Omega_j(\xi)) \\ &- \frac{E_p h_p}{1 - \upsilon_p^2} T(\psi^k) \sum_{j=1}^{M} a_{pj} \int_0^{R_p} \left(\frac{\partial \psi}{\partial \xi}\right)\Big|_{w=w^k} \left(\frac{\partial \Omega}{\partial \xi}\right) d\xi \\ &= -\sum_{i=1}^{N} 2\pi H^k \int_0^{R_m} a_{mi}\mu_i(r) r dr \\ &+ \sum_{j=1}^{M} 2\pi H^k \int_0^{R_p} a_{pj}\Omega_j(\xi)\xi d\xi + E_2 \end{aligned} \tag{30}$$

where $E_1$ and $E_2$ are residuals or errors related to the approximation by the finite space function. Applying the Galerkin method, the integral of the weighted residuals over the membrane and plate domains ($0 - R_m$ for Eq. (29) and $0 - R_p$ for Eq. (30)) are forced to zero. Therefore, we have:

$$\sum_{i=1}^{N}\int_{0}^{R_m} D_m\mu_{jj}(r)L(a_{mi}\mu_i(r))dr$$
$$-\sum_{i=1}^{N}\int_{0}^{R_m} N_{am}^{k}\mu_{jj}(r)T(a_{mi}\mu_i(r))\,dr$$
$$-\sum_{i=1}^{N}\int_{0}^{R_m} a_{mi}\left(\frac{E_m h_m}{1-\upsilon_m^2}T(w^k)\int_{0}^{R_m}\left(\frac{\partial w}{\partial r}\right)\Big|_{w=w^k}\left(\frac{\partial \mu}{\partial r}\right)dr\right)dr \quad (31)$$
$$=-\sum_{i=1}^{N}\int_{0}^{R_m}\mu_{jj}(r)\left(2\pi H^k\int_{0}^{R_m} a_{mi}\mu_i(r)r dr\right)dr$$
$$+\sum_{j=1}^{M}\int_{0}^{R_m}\mu_{jj}(r)\left(2\pi H^k\int_{0}^{R_p} a_{pj}\Omega_j(\xi)\xi d\xi\right)dr$$
$$+\int_{0}^{R_m}\mu_{jj}(r)\Delta\hat{P}_{in}dr$$

$$\sum_{j=1}^{M}\int_{0}^{R_p} D_p\Omega_{ii}(\xi)L(a_{pj}\Omega_j(\xi))\,d\xi$$
$$-\sum_{j=1}^{M}\int_{0}^{R_p} N_{ap}^{k}\Omega_{ii}(\xi)\,T(a_{pj}\Omega_j(\xi))d\xi$$
$$-\sum_{j=1}^{M}\int_{0}^{R_p}\Omega_{ii}(\xi)a_{pj}\frac{E_p h_p}{1-\upsilon_p^2}T(\psi^k)\left(\int_{0}^{R_p}\left(\frac{\partial \psi}{\partial \xi}\right)\Big|_{w=w^k}\left(\frac{\partial \Omega}{\partial \xi}\right)d\xi\right)d\xi \quad (32)$$
$$=-\sum_{i=1}^{N}\int_{0}^{R_p}\Omega_{ii}(\xi)\left(2\pi H^k\int_{0}^{R_m} a_{mi}\mu_i(r)r dr\right)d\xi$$
$$+\sum_{j=1}^{M}\int_{0}^{R_p}\Omega_{ii}(\xi)\left(2\pi H^k\int_{0}^{R_p} a_{pj}\Omega_j(\xi)\xi d\xi\right)d\xi$$

It should be noted that equations (31) and (32) are multiplied into $\mu_{jj}(r)$ and $\Omega_{ii}(\xi)$, respectively.

Solving this set of algebraic equations (with $(M+N)$ unknown variables and $(M+N)$ equations) for each step, the static changes in deflection for the membrane and sensing plate are obtained.

## VI. Results and Discussion

This section presents the results obtained from modeling the piezoresistive-type pressure transmitter shown in figure (1). Table (1) provides a summary of the variables and their corresponding values used to generate the numerical results. Note that other variables mentioned in the following text are shown in figure (1b). As stated above, the main focus of this paper is on the effects of oil loss on the static behavior of the pressure sensor. Accordingly, our simulation results examine the effects of trapped gas (assumed to be air) on the deflection of the plates (i.e. the maximum displacement occurring at $r=0$ and $\xi=0$), the maximum measurable pressure (MMP) and the sensor sensitivity.

***Table 1:*** *Simulation variables and selected values.*

| | | |
|---|---|---|
| Geometry parameters | | |
| Membrane radius | $R_m$ | |
| Middle hole radius | $R_h$ | $0.56\ mm$ |
| Plate radius | $R_p$ | |
| Thickness of the membrane | $h_m$ | $0.04\ mm$ |
| Thickness of the plate | $h_p$ | $0.3\ mm$ |
| Height of upper cylinder | $h_{u0}$ | $0.1\ mm$ |
| Height of the middle cylinder (hole between upper and lower cylinders) | $h_h$ | $32\ mm$ |
| Height of lower cylinder | $h_{l0}$ | $0.3\ mm$ |
| Thickness of air film when no pressure is applied | $g_{air}$ | |
| Material properties | | |
| Young's modulus of membrane | $E_m$ | $205\ Gpa$ |
| Young's modulus of plate | $E_p$ | $205\ Gpa$ |
| Poisson's ratio of membrane | $\upsilon_m$ | 0.3 |
| Poisson's ratio of plate | $\upsilon_p$ | 0.3 |
| Universal gas constant | $\bar{R}$ | $8.314\ {}^{J}/_{mol.K}$ |

Figure (2) illustrates the sensor output (maximum deflection of the sensing plate) and the membrane displacement as a function of the applied pressure for different values of oil loss. The variable % Oil-Loss indicates the percentage by volume of oil lost due to the leakage fault, so that 0% oil-loss is the fault-free condition.

The simulation results suggest that, with any gas present, the behavior of the membrane is quite nonlinear, while the sensor output still behaves linearly. However, increasing the amount of air in the interface volume leads to the reduction in the linear range of the pressure measured by the sensor before output saturation occurs.

The sensor output remains linear despite the presence of air and non-linear behavior of the membrane, because the sensing plate is much stiffer than the membrane. As a result, the main interaction is between the softer membrane and the air volume. With higher air content, the membrane displacement becomes increasingly sensitive to applied pressure, but once displacement reaches its limit, no further transmission of pressure to the sensing plate is possible, and the sensor output saturates.

In other simulations, the sensor output shows nonlinear behavior when the stiffness of the sensing plate is similar to that of the membrane. In this situation, the sensor behaves poorly for low applied pressure (since plate is much stiffer than air) resulting in a very low MMP. Accordingly, the material and geometry parameters should be selected to ensure that any output nonlinearity is limited and that the MMP remains within a reasonable range.

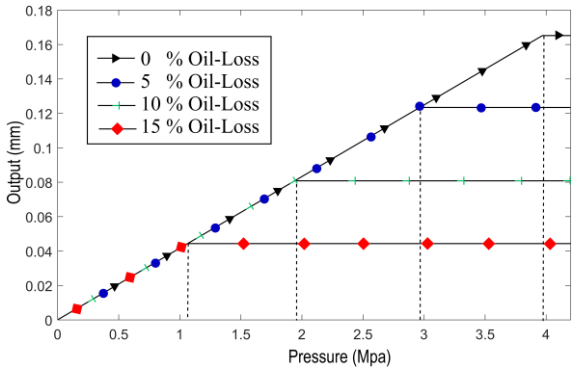


(a)

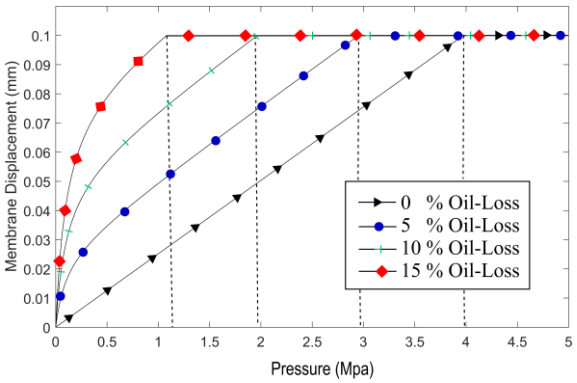


(b)

***Fig 2:*** *The variations of the sensing plate and membrane displacement (center point) versus input pressure for different levels of Oil-Loss.* $R_m = 9\ mm$ , $R_p = 7\ mm$.

From the structure of the pressure sensor (figure (1a)), it can be understood that the MMP is restricted by the maximum permitted displacement of the membrane, based on the geometry ($h_{u0}$) and the elastic limit (avoiding plastic deformation). Accordingly, the MMP is a key performance metric when considering the impact of oil loss faults and its interaction with sensor design parameters. For example, Figure (3) shows the relationship between the MMP and the oil loss percentage, for different membrane radii. It can be seen that the impact of oil loss on MMP is strongly influenced by the geometry of the sensor design.

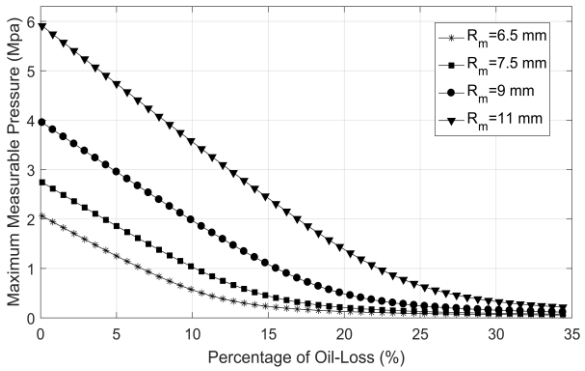


***Fig 3****: Variations of the MMP as a function of the percentage of filler oil for different membrane radii.*

Sensitivity is another important concept in the design and analysis of sensors. The sensitivity is usually defined as the change in the sensor output per unit change in the sensor input [35]. As shown in figure (4), loss of filler oil results in a drop in the sensitivity of the pressure sensor, demonstrating once again the importance of preventing and/or detecting the introduction of air into the filling oil.

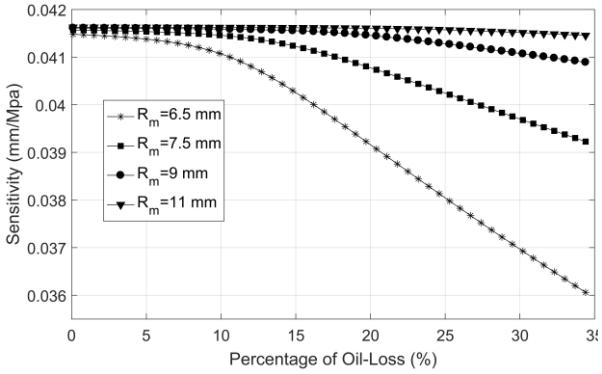


***Fig 4****: The sensitivity of the sensor versus percent of filler oil for different membrane radius.*

## VI. Conclusion

In this paper, the main failures modes of the piezoresistive-type pressure sensors were discussed. The failures were divided into four categories: temperature effects, corrosion, oil loss and pressure discharge. For the cases of temperature-related faults and oil loss, mathematical models were proposed, with solutions derived for oil loss. The nonlinear governing equations were linearized using the SSL method, and then the Galerkin-based residual method was used to solve the resulting linear equations for each increasing pressure step. The simulated behavior with oil-loss was reported for three of the main parameters for strain gauge type pressure transducers: the sensor output, the MMP and the sensitivity.

## References

[1] M.B. Moran, Michael J. ; Shapiro, Howard N. ; Boettner, Daisie D. ; Bailey, Fundamentals of Engineering Thermodynamics, CRC Press, 2019.

[2] M.M. Nayak, N. Gunasekaran, K. Rajanna, S. Srinivasulu, S. Mohan, The Strain Gauge Pressure Transducers—An Overview, IETE Tech. Rev. 9 (1992) 170–177.

[3] E.G. Bakhoum, M.H.M. Cheng, Capacitive Pressure Sensor With Very Large Dynamic Range, IEEE Trans. Components Packag. Technol. 33 (2010) 79–83..

[4] J. Yang, Y. Ye, X. Li, X. Lü, R. Chen, Flexible, conductive, and highly pressure-sensitive graphene-polyimide foam for pressure sensor application, Compos. Sci. Technol. 164 (2018) 187–194.

[5] D. Tandeske, Pressure sensors: Selection and Application, New York: M, (1991).

[6] S.S. Kumar, B.D. Pant, Erratum to: Design principles and considerations for the 'ideal' silicon piezoresistive pressure sensor: a focused review, Microsyst. Technol. 20 (2014) 2303–2303.

[7] T. Xu, L. Zhao, Z. Jiang, X. Guo, J. Ding, W. Xiang, Y. Zhao, A high sensitive pressure sensor with the novel bossed diaphragm combined with peninsula-island structure, Sensors Actuators A Phys. 244 (2016) 66–76. https://doi.org/10.1016/j.sna.2016.04.027.

[8] Y. Yang, H. Pan, G. Xie, Y. Jiang, C. Chen, Y. Su, Y. Wang, H. Tai, Flexible piezoelectric pressure sensor based on polydopamine-modified BaTiO3/PVDF composite film for human motion monitoring,

Sensors Actuators A Phys. 301 (2020) 111789. https://doi.org/10.1016/j.sna.2019.111789.
[9] Y. Seo, D. Kim, N.A. Hall, High-Temperature Piezoelectric Pressure Sensors for Hypersonic Flow Measurements, in: 2019 20th Int. Conf. Solid-State Sensors, Actuators Microsystems Eurosensors XXXIII (TRANSDUCERS EUROSENSORS XXXIII), IEEE, 2019: pp. 2110–2113. https://doi.org/10.1109/TRANSDUCERS.2019.8808755.
[10] L. Zhao, L. Huang, G. Luo, J. Wang, H. Wang, Y. Wu, Z. Li, X. Zhou, Z. Jiang, An immersive resonant sensor with microcantilever for pressure measurement, Sensors Actuators A Phys. 303 (2020) 111686. https://doi.org/10.1016/j.sna.2019.111686.
[11] Y. Li, Y. Lu, B. Xie, J. Chen, J. Wang, D. Chen, A Micromachined Resonant Differential Pressure Sensor, IEEE Trans. Electron Devices. 67 (2020) 640–645. https://doi.org/10.1109/TED.2019.2957880.
[12] Q. Cui, P. Thakur, C. Rablau, I. Avrutsky, M.M.-C. Cheng, Miniature Optical Fiber Pressure Sensor With Exfoliated Graphene Diaphragm, IEEE Sens. J. 19 (2019) 5621–5631. https://doi.org/10.1109/JSEN.2019.2904020.
[13] S. Choi, S.-L. Lee, J. Kim, S.J. Jeong, M.S. Kim, D. Kim, Y.W. Lee, High Sensitivity Polarimetric Optical Fiber Pressure Sensor Based on Tapered Polarization-Maintaining and Fiber Bragg Grating, J. Nanosci. Nanotechnol. 19 (2018) 1403–1409. https://doi.org/10.1166/jnn.2019.16190.
[14] S. Zhang, L. Zhang, L. Wang, F. Wang, G. Pan, A Flexible e-skin based on micro-structured PZT thin films prepared via a low-temperature PLD method, J. Mater. Chem. C. 7 (2019) 4760–4769. https://doi.org/10.1039/C8TC06350H.
[15] H. Wei, H. Wang, Y. Xia, D. Cui, Y. Shi, M. Dong, C. Liu, T. Ding, J. Zhang, Y. Ma, N. Wang, Z. Wang, Y. Sun, R. Wei, Z. Guo, An overview of lead-free piezoelectric materials and devices, J. Mater. Chem. C. 6 (2018) 12446–12467. https://doi.org/10.1039/C8TC04515A.
[16] M.G. Xu, H. Geiger, J.P. Dakin, Fibre grating pressure sensor with enhanced sensitivity using a glass-bubble housing, Electron. Lett. 32 (1996) 128. https://doi.org/10.1049/el:19960022.
[17] J.W. Arkwright, I.D. Underhill, S.A. Maunder, A. Jafari, N. Cartwright, C. Lemckert, Fiber Optic Pressure Sensing Arrays for Monitoring Horizontal and Vertical Pressures Generated by Traveling Water Waves, IEEE Sens. J. 14 (2014) 2739–2742. https://doi.org/10.1109/JSEN.2014.2311806.
[18] J. Xu, X. Wang, K.L. Cooper, A. Wang, Miniature all-silica fiber optic pressure and acoustic sensors, Opt. Lett. 30 (2005) 3269. https://doi.org/10.1364/OL.30.003269.
[19] D. Zhang, M. Wang, Z. Yang, Facile fabrication of graphene oxide/Nafion/indium oxide for humidity sensing with highly sensitive capacitance response, Sensors Actuators B Chem. 292 (2019) 187–195. https://doi.org/10.1016/j.snb.2019.04.133.
[20] Y.M. Sabry, D. Khalil, T. Bourouina, Monolithic silicon-micromachined free-space optical interferometers onchip, Laser Photon. Rev. 9 (2015) 1–24. https://doi.org/10.1002/lpor.201400069.
[21] B.R. Burg, T. Helbling, C. Hierold, D. Poulikakos, Piezoresistive pressure sensors with parallel integration of individual single-walled carbon nanotubes, J. Appl. Phys. 109 (2011) 064310. https://doi.org/10.1063/1.3555619.
[22] H.H. Tsai, C.C. Hsieh, C.W. Fan, Y.C. Chen, W. Te Wu, Design and characterization of temperature-robust piezoresistive micro-pressure sensor with double-wheatstone-bridge structure, in: DTIP MEMS MOEMS - Symp. Des. Test, Integr. Packag. MEMS/MOEMS, IEEE, 2009: pp. 363–368.
[23] Shuang Chen, Ming-quan Zhu, Bing-he Ma, Wei-zheng Yuan, Design and optimization of a micro piezoresistive pressure sensor, in: 2008 3rd IEEE Int. Conf. Nano/Micro Eng. Mol. Syst., IEEE, 2008: pp. 351–356. https://doi.org/10.1109/NEMS.2008.4484350.
[24] J.J.T. Steve Cho, Y. Zhang, K. Najafi, K.D.K.D. Wise, J. Ji, S.T. Cho, Y. Zhang, K. Najafi, K.D.K.D. Wise, An Ultraminiature CMOS Pressure Sensor for a Multiplexed Cardiovascular Catheter, IEEE Trans. Electron Devices. 39 (1992) 2260–2267. https://doi.org/10.1109/16.158797.
[25] Y.-H. Zhang, C. Yang, Z.-H. Zhang, H.-W. Lin, L.-T. Liu, T.-L. Ren, A Novel Pressure Microsensor With 30-$\mu \hbox{m}$-Thick Diaphragm and Meander-Shaped Piezoresistors Partially Distributed on High-Stress Bulk Silicon Region, IEEE Sens. J. 7 (2007) 1742–1748. https://doi.org/10.1109/JSEN.2007.910298.
[26] A.A. Barlian, W.-T. Park, J.R. Mallon, A.J. Rastegar, B.L. Pruitt, Review: Semiconductor Piezoresistance for Microsystems., Proc. IEEE. Inst. Electr. Electron. Eng. 97 (2009) 513–552. https://doi.org/10.1109/JPROC.2009.2013612.
[27] G. Rezazadeh, A. Tahmasebi, M. Zubstov, Application of piezoelectric layers in electrostatic MEM actuators: controlling of pull-in voltage, Microsyst. Technol. 12 (2006) 1163–1170. https://doi.org/10.1007/s00542-006-0245-5.
[28] R. Shabani, H. Hatami, F.G. Golzar, S. Tariverdilo, G. Rezazadeh, Coupled vibration of a cantilever micro-beam submerged in a bounded incompressible fluid domain, Acta Mech. 224 (2013) 841–850. https://doi.org/10.1007/s00707-012-0792-z.
[29] G. Rezazadeh, M. Fathalilou, M. Sadeghi, Pull-in voltage of electrostatically-actuated microbeams in terms of lumped model pull-in voltage using novel design corrective coefficients, Sens. Imaging. 12 (2011) 117–131. https://doi.org/10.1007/s11220-011-0065-2.
[30] E.A. Thornton, Thermal Buckling of Plates and Shells, Appl. Mech. Rev. 46 (1993) 485–506. https://doi.org/10.1115/1.3120310.
[31] L.H. Wu, L. Bin Wang, S.H. Liu, Thermal buckling of a simply supported rectangular FGM plate, Gongcheng Lixue/Engineering Mech. 21 (2004) 152-156+166.
[32] D. Coffin, F. Bloom, Hygrothermal buckling and bending of thin plates. Project F020, report 4 to the member companies of the Institute of Paper Science and Technology, (1998).
[33] S.S. Rao, Vibration of Continuous Systems, John Wiley & Sons, Inc., Hoboken, NJ, USA, 2006. https://doi.org/10.1002/9780470117866.
[34] G. Rezazadeh, M. Fathalilou, R. Shabani, S. Tarverdilou, S. Talebian, Dynamic characteristics and forced response of an electrostatically-actuated microbeam subjected to fluid loading, Microsyst. Technol. 15 (2009) 1355–1363. https://doi.org/10.1007/s00542-009-0906-2.